

Sensory attenuation develops as a result of sensorimotor experience

Hayato Idei¹, Wataru Ohata², Yuichi Yamashita³, Tetsuya Ogata¹ and Jun Tani^{2*}

¹Department of Intermedia Art and Science, Waseda University, Tokyo, Japan

²Cognitive Neurorobotics Research Unit, Okinawa Institute of Science and Technology, Okinawa, Japan

³Department of Information Medicine, National Center of Neurology and Psychiatry, Tokyo, Japan

*Correspondence to: jun.tani@oist.jp

December 2, 2021

Abstract

The brain attenuates its responses to self-produced exteroceptions (e.g., we cannot tickle ourselves) (*1*). Is this phenomenon, known as sensory attenuation, enabled innately, or is it acquired through learning? For decades, theoretical and biological studies have suggested related neural functions of sensory attenuation, such as an efference copy of the motor command (*2, 3*) and neuromodulation (*4*); however, the developmental aspect of sensory attenuation remains unexamined. Here, our simulation study using a recurrent neural network, operated according to a computational principle called free-energy minimization (*5*), shows that sensory attenuation can be developed as a free-energy state in the network through learning of two distinct types of sensorimotor patterns, characterized by self-produced or externally produced exteroceptive feedback. Simulation of the network, consisting of sensory (proprioceptive and exteroceptive), association, and executive areas, showed that shifts between these two types of sensorimotor patterns triggered transitions from one free-energy state to another in the network. Consequently, this induced shifts between attenuating and amplifying responses in the sensory areas. Furthermore, the executive area, proactively adjusted the precision of the prediction in lower levels while being modulated by the bottom-up sensory prediction error signal in minimizing the free-energy, thereby serving as an information hub in generating the observed shifts. We also found that innate alterations in modulation of sensory-information flow induced some characteristics analogous to schizophrenia and autism spectrum disorder. This study provides a novel perspective on neural mechanisms underlying emergence of perceptual phenomena and psychiatric disorders.

Introduction:

The brain couples its structure with the outside world via sensorimotor experiences (6). A posteriori development of neural processing gradually forms our perceptual phenomena, with a priori nature determined by genes. It yields well-defined self-experience and helps to confidently situate self in relation to others. In general, we face two primary types of sensorimotor experience, self-movements and sensory events in the outside world, which may or may not be correlated. Recognition of the difference is thought to underlie self-other distinction or sense of self (7, 8), but the difference cannot be known a priori. The brain may acquire the capacity to modulate neural responses via sensorimotor learning, depending on the condition.

A phenomenon called sensory attenuation, is recognized as one of the bases of the sense of self, especially the sense of agency (7, 9). Sensory attenuation refers to an experience in which an exteroception produced by a self-movement is less salient than one produced externally (1). A perfect example is the difficulty of tickling ourselves. In addition, the ability to ignore visual changes during eye or head movements is thought to help maintain stability of the visual scene. At the neural level, sensory attenuation is observed as reduced brain responses, such as blood oxygen level-dependent (BOLD) responses, especially in sensory areas (10–12). A line of research shows that sensory attenuation is associated with predicted sensorimotor correlation and is diminished by temporal or spatial mismatch between a movement and the resultant exteroception (e.g., a temporal delay) (3, 13, 14). There are some suggestions of underlying neural functions, such as an efference copy of the motor command (2, 3) and neuromodulation (e.g., dopaminergic transmission) (4). However, despite intensive work for decades, a fundamental question remains unexamined: Is sensory attenuation enabled innately or is it acquired through learning? The latter possibility remains almost entirely unexplored, although increased sensory attenuation with age is observed in adults (15).

Here, we provide a novel mechanistic explanation, suggesting that sensory attenuation can be self-organized through learning. We focus on the following factors. If a self-movement and a sensory event in the outside world are not correlated, the resultant proprioception and exteroception occur separately. The brain may efficiently use individual sensory areas to process these individual sensations. On the other hand, if the proprioception and exteroception are correlated, they can be perceived as coupled, rather than individual sensations. In that case, it is reasonable to process the sensorimotor coupling using an association area, and neural responses in individual sensory areas can be attenuated. That is, through sensorimotor learning, the brain may develop the capacity to modulate sensory-information flow and processing inside the hierarchical neural networks, depending on the conditions. To test this hypothesis, we conducted a robotic simulation experiment using a variational recurrent neural network (RNN) model based on Bayesian brain theory or free-energy minimization (5, 6, 16–18).

Results:

Computational model

Our daily sensorimotor behavior generally has some sort of regularity (e.g., a set-point of body posture and dynamic movement patterns) and randomness (e.g., free movement with fluctuations) (19). Therefore, we considered how a robot agent controlled by an RNN develops sensory attenuation through such spontaneous sensorimotor experiences (Fig. 1). A robot repeatedly generated a random behavior and then returned to the set-posture within five seconds (20 time steps for the robot), where the robot’s motion and a movement of an external red object were correlated (self-produced condition) or uncorrelated (externally produced condition). The received sensations were 3-dimensional proprioception for joint angles and 2-dimensional exteroception for the position of the object. Previous brain imaging studies show that sensory attenuation involves hierarchical interactions among multiple brain regions, including sensory areas, an association area (parietal area), and a higher cognitive area (prefrontal or supplementary motor area) (15, 20, 21). The RNN inside the robot has a corresponding hierarchical structure, referred to as sensory (exteroceptive and proprioceptive), association, and executive areas (Fig. 1a). The hierarchical RNN is a generative model that predicts sensations as well as inferring hidden causes of sensations via free-energy minimization (17, 18). Each area has individual latent variables z_t representing each level of belief about the hidden cause of sensation in the form of Gaussian distributions. Each latent variable has prior z_t^p and posterior z_t^q distributions that correspond to estimated hidden causes before and after observing sensations, respectively. The priors and posteriors of latent variables are time-varying in sensory and association areas, while the executive area maintains a constant posterior state during sequential prediction generation within a time window (Extended Data Fig. 1-2). We assumed that the executive area controls (and switches) sequential patterns of lower-level network behavior, like the prefrontal or supplementary motor area in a biological brain (22, 23). At each time step, the RNN generates predictions \hat{x}_t about the next exteroceptive and proprioceptive sensations x_t from latent variables via recurrent units d_t , representing dynamics of the environment. Free-energy F_t can be calculated as the sum of prediction error and Kullback-Leibler divergence between the posterior and prior at each l th network level.

$$F_t = \underbrace{\frac{1}{2} (x_t - \hat{x}_t)^2}_{\text{Prediction error}} + \sum_{l=1}^3 W^{(l)} \underbrace{D_{KL}[q(z_t^{(l)} | e_{t:T}) || p(z_t^{(l)} | d_{t-1}^{(l)})]}_{\text{Influence of prior beliefs}}.$$

This describes integration of sensory information (i.e., prediction error e_t) and prior knowledge (i.e., prior belief z_t^p) upon a posterior z_t^q update, although synaptic weights are also updated during the learning process. A posterior is only adjusted to minimize prediction errors under the influence of the prior. A weak prior (with low precision) leads to a sensitive posterior update in response to a prediction error, while a strong prior (with high precision) leads to discounting of the prediction error. In other words, prediction error flows into (or is minimized by adjusting the posterior) in the presence of a weak prior. The strength of the prior in each area is represented in two ways. First, it is dynamically modulated as the estimated sigma (inverse precision) of the

prior distribution, which is self-organized during the learning process. From available physiological evidence, it may engage neuromodulators, such as acetylcholine and dopamine (5, 24). In addition, we introduce a hyper-parameter called the meta-prior $W^{(l)}$, which controls the meta-level balance between the prediction error and the divergence between the posterior and the prior at each network level. Previous studies have shown that a large meta-prior causes an intrinsically strong prior, whereas a small meta-prior causes an intrinsically weak prior (17, 18). We assumed that the meta-prior represents an innately equipped characteristic in the biological brain. In the baseline model, we set the meta-prior to the same value for all network levels ($W^{(1)} = W^{(2)} = W^{(3)} = 0.005$) to avoid bias in the prediction-error flow.

Emergence of sensory attenuation

The experiment comprises learning and test phases. In the learning phase, the robot learned to reproduce the two types of sensorimotor patterns (Fig. 1b). Target sensorimotor sequences were prepared in advance from human spontaneous behaviors through manual manipulations of a physical robot. We prepared 24 training sets for each set of self-produced and externally produced conditions. We ensured that the total number of movements was the same for both conditions. The RNN updated posteriors and synaptic weights to minimize the free-energy (Extended Data Fig. 1).

In the test phase, the trained robot was required to generate actions by itself and to recognize an environmental condition by updating only posteriors to minimize the free-energy, with fixed synaptic weights (Fig. 2a and Extended Data Fig. 2). Action generation of the robot was performed by proportional-integral-derivative (PID) control. A PID controller receives proprioceptive predictions as target joint angles and it changes the joint angles (proprioception) to minimize the error between the current state and target. In this regard, it implements the thought of active inference in the free-energy principle (16). Fig. 2b-e shows an example of a test trial performed by the baseline model (Supplementary Video 1). The test trial consists of a self-produced condition during time steps 0-100 and an externally produced condition during time steps 100-200.

In the self-produced condition, the robot moved the external object by itself, and the object position matched the robot’s hand position (Fig. 2e). The trained RNN successfully reproduced the stochastic property of learned sensorimotor sequences by modulating the association-level latent mean $\mu^{(2)}$, such that the estimated sigma $\sigma^{(2)}$ was high during random behavior generation, but low when returning to the set-posture (Fig. 2c). On the other hand, modulation of the latent mean in exteroceptive and proprioceptive areas $\mu^{(1)}$ was small, with low estimated sigma $\sigma^{(1)}$ (Fig. 2d), suggesting reduced prediction-error flow into sensory areas with high precision in its prior. These results indicate that the RNN minimized prediction errors produced by self-movements mainly by adjusting the posterior in the association area, since the posterior in sensory areas cannot be easily adjusted because of the strong prior.

Then, at time step 100, the environment was shifted to externally produced conditions, where the object position was given from test data that were not used in the learning phase. The object position and hand position became uncorrelated (Fig. 2e). The environmental change caused a stepwise change in the executive-level latent state $\mu^{(3)}$ (Fig. 2b). At the same time, in sensory areas, modulation in the latent mean $\mu^{(1)}$

was amplified and sigma $\sigma^{(1)}$ increased, showing periodic modulation (Fig. 2d), like the association-level latent state. This shows that the RNN minimized prediction errors from externally produced sensations by adjusting the posterior in sensory areas, as well as in the association area.

Collectively, the hierarchical RNN attenuated neural responses in sensory areas for the self-produced condition and amplified them for the externally produced condition by proactively controlling the precision of the prior at each network level, in which the posterior in the executive area worked as the information hub for switching the lower-level precision structure and the prediction error flow (Fig. 3). Furthermore, the free-energy converged into different states for distinct sensorimotor conditions (Fig. 3). This suggests that a particular global free-energy minimum was developed for each sensorimotor condition and the transition of the free-energy state in the network, induced by the abrupt condition shift, underlay the qualitative change in the free-energy minimization.

For quantitative analysis, we prepared 10 trained networks with different initial synaptic weights and conducted 8 test trials for each trained network. Fig. 4a shows the change in the sensory-level posterior mean $\mu^{(1),q}$ per time step for the two conditions. In this study, it is referred to as a sensory-level posterior response. A paired t-test reported that the posterior response was significantly smaller in the self-produced condition than in the externally produced condition ($t(9) = -3.38, p = 0.0082$). In addition, a paired t-test showed that the sensory-level prior sigma $\sigma^{(1),p}$ in the self-produced condition was significantly lower than that in the externally produced condition ($t(9) = -3.32, p = 0.0089$) (Fig. 4b).

Furthermore, we analyzed how attenuation of neural responses in sensory areas developed during the learning process. The RNN first increased sensory-level posterior responses to reconstruct target sensorimotor sequences (Fig. 4c). Then, sensory-level posterior responses in the self-produced condition were gradually attenuated in both exteroceptive and proprioceptive areas. The sensory-level prior sigma diminished more in the self-produced condition than in the externally produced condition through the learning process (Fig. 4d). We confirmed that posterior responses in the association area were similar in self-produced and externally produced conditions (Extended Data Fig. 3a-b), indicating reduced total neural response in the self-produced condition. This sensory attenuation was accompanied by recognition of both conditions in the executive area (Extended Data Fig. 3c-d). These results demonstrate emergence of sensory attenuation through a learning process via free-energy minimization. Additional analyses indicated that development of sensory attenuation was diminished by removing neurons in the association or executive area (Extended Data Fig. 4), suggesting the importance of a higher-level representation of sensorimotor correlation.

Discussion:

The current model study, using a hierarchically organized variational RNN, illustrated the possibility that the mechanism for sensory attenuation can be developed through learning instead of being innate. For dealing with two distinct types of sensorimotor conditions, namely self-produced and externally produced conditions, the network

developed two distinct free-energy states through learning, wherein each free-energy state corresponds to each sensorimotor condition (Fig. 3 and 4c-d). In the developed network, the top-down and bottom-up pathways functioned as follows. In the top-down pathway, the posterior in the executive area predicted the prior precision of the association area and the sensory areas. In the bottom-up pathway, prediction error determined the posterior of the sensory areas, the association area, and the executive area under the constraint of the prior precision expected at each area by the top-down pathway. Here, we see that the top-down pathway and the bottom-up pathway created a closed circuit wherein the posterior in the executive area served as the information hub.

In the self-produced condition, sensory attenuation was achieved by minimizing the free-energy to the corresponding free-energy state. In this condition, the posterior in the executive area developed to a particular value induced high prior precision in sensory areas and low prior precision in the association area, which resulted in less adaptation in its posterior in sensory areas and more adaptation in the association area using the bottom-up error signal. Less adaptation in the posterior in sensory areas corresponds to sensory attenuation. The error bottom-up to the executive area determined the posterior in the executive area with its prior set to a neutral value.

In the externally produced condition, the process went the other way around, wherein the posterior in sensory areas adapted greatly because of the low precision in its prior regulated by the executive area. This corresponds to sensory amplification. The change of the sensorimotor condition triggered the transition from one free-energy state to another one, i.e., from sensory attenuation to sensory amplification and verse-versa.

There have been prior model proposals to account for sensory attenuation. One proposal (4) explains that sensory attenuation is caused by reducing the precision of the prediction error bottom-up to the sensory area by following the free-energy principle. This model, however, does not explain the involvement of the higher executive area, as evidenced by (15, 20). We confirmed that removal of the executive area diminished the development of sensory attenuation (Extended Data Fig. 4b), emphasizing the contribution of the frontal function. This is consistent with biological studies suggesting that signals from the frontal area, such as the supplementary motor area, predictively control the intensity of sensations. Their disruption causes diminished sensory attenuation (20, 25).

According to another leading hypothesis, the pathway of an efference copy of the motor command is thought to originate from top-down signals (20, 25). On the other hand, our model suggests that signals from the executive (frontal) area may represent predictive signals for controlling prediction-error flow inside the hierarchical network, rather than a copy of the motor command. To our knowledge, the self-organized functionality, in which top-down signals hierarchically control bottom-up prediction-error flow into each local area (that modulates top-down signals), is reported here for the first time. In addition, development of distinct free-energy states in the network through learning provides new insights into emergence of perceptual phenomena.

The perspective that sensory attenuation is a consequence of learning instead of an innate function, may be indirectly supported by a recent study suggesting that a target stimulus of sensory attenuation can be adaptively changed through rapid learning (26). In addition, our result (Fig. 4c) explains increased sensory attenuation with age in adults (15). Furthermore, our model suggests that proprioception, as well as

exteroception, can be attenuated when a self-movement produces exteroception. In fact, a neuroimaging study observes less cerebellar activity when a movement produces a tactile stimulus, than when it does not (10).

In supplementary results, we simulated a variety of innate alterations in modulation of prediction-error flow by manipulating the meta-prior at each network level (see Supplementary Information and Extended Data Fig. 5-9 for details). The results show that innately decreased and increased prediction-error flow into the association area induced some sets of characteristics analogous to schizophrenia (i.e., reduced sensory attenuation and delusion) (3, 4, 27, 28) and autism spectrum disorder (i.e., reduced generalization, cognitive inflexibility, and normally developed sensory attenuation) (29–32), respectively. This raises the possibility that a mechanistic difference between schizophrenia and autism spectrum disorder can be explained by alterations in the predictive control of prediction-error flow. This study may serve as a step toward building a brain-inspired (minimal) sentient machine with or without psychiatric disorders.

Acknowledgments:

Funding: This work was partially supported by an unrestricted gift from Google and supported by a JSPS Grant-in-Aid (No. JP19J20281), JST Moonshot R&D (No. JPMJMS2031), and JST CREST grants (Nos. JPMJCR16E2, JPMJCR21P4).

Competing interests: Authors declare that they have no competing interests.

Data and materials availability: All data is available in the manuscript or the supplementary materials. Computer code for the neural network model was written by using Pytorch (a library for deep learning) and is available online (https://github.com/h-idei/pvrnn_sa.git).

Supplementary Methods

Neural network model

To simulate development of sensory attenuation, we utilized a predictive-coding-inspired variational recurrent neural network (PV-RNN), which represents a generative process of sensation from a hidden cause in the environment, based on the free-energy principle (FEP) (17, 18). It consists of sensory (exteroceptive and proprioceptive), association, and executive areas, in which there are deterministic neurons and latent (stochastic) neurons. Latent neurons represent belief of the cause of sensation as Gaussian distributions (for simplicity). Each latent state has prior and posterior probability distributions that correspond to estimated hidden causes before and after observing sensations, respectively. Based on the latent states, the PV-RNN generates predictions about next sensations in a top-down way. Here, deterministic neurons transform latent states into sensory predictions via synaptic connections that represent relationships between sensations and their causes. The PV-RNN uses a multiple timescale RNN (MTRNN) (33) as the transformation function. An RNN represents temporal processing of the brain in that neural activity is determined by the past history of neural states. Owing to their capacity to learn to reproduce complex dynamic behaviors, RNNs have been used in computational modeling and developmental neurobotic studies to understand cortical processing and cognitive functions, including psychiatric symptoms (33–35). In addition, MTRNNs have a multiple timescale property in neural activation, which enables them to represent a temporal hierarchy in the environment, as observed in the biological brain (36). By using a PV-RNN, we can consider complex sensorimotor behaviors that have both temporal regularity and stochasticity (17, 18). To perform spontaneous behaviors like daily human behaviors, a neural network controlling robot was required to process short-term random movements and a long-term periodic pattern, as in the experiment in which the multiple timescale property is thought to facilitate sensorimotor learning. In the following sections, we describe the mathematical details of top-down prediction generation and bottom-up parameter updates by the PV-RNN (Extended Data Fig. 1-2).

Prediction generation

Prediction generation is performed in a top-down way through the network hierarchy. The internal state $h_{t,i}^{(s)}$ and output $d_{t,i}^{(s)}$ of the i th deterministic neuron of the s th target

sequence at time step t ($t \geq 1$) is calculated as

$$h_{t,i}^{(s)} = \begin{cases} \frac{1}{\tau} \left(\sum_{j \in I_{Ad}} w_{ij} d_{t-1,j}^{(s)} + \sum_{j \in I_{Az}} w_{ij} z_{t,j}^{(s)} + \sum_{j \in I_{Cz}} w_{ij} z_{t,j}^{(s)} + b_i \right) + \left(1 - \frac{1}{\tau} \right) h_{t-1,i}^{(s)} & (i \in I_{Ad}), \\ \frac{1}{\tau} \left(\sum_{j \in I_{Ed}} w_{ij} d_{t-1,j}^{(s)} + \sum_{j \in I_{Ez}} w_{ij} z_{t,j}^{(s)} + \sum_{j \in I_{Ad}} w_{ij} d_{t,j}^{(s)} + b_i \right) + \left(1 - \frac{1}{\tau} \right) h_{t-1,i}^{(s)} & (i \in I_{Ed}), \\ \frac{1}{\tau} \left(\sum_{j \in I_{Pd}} w_{ij} d_{t-1,j}^{(s)} + \sum_{j \in I_{Pz}} w_{ij} z_{t,j}^{(s)} + \sum_{j \in I_{Ad}} w_{ij} d_{t,j}^{(s)} + b_i \right) + \left(1 - \frac{1}{\tau} \right) h_{t-1,i}^{(s)} & (i \in I_{Pd}). \end{cases} \quad (1)$$

$$d_{t,i}^{(s)} = \tanh \left(h_{t,i}^{(s)} \right) \quad (i \in I_{Ed}, I_{Pd}, I_{Ad}). \quad (2)$$

Here, I_{Ed} , I_{Pd} , and I_{Ad} are index sets of deterministic neurons in the exteroceptive area, proprioceptive area, and association area, respectively. I_{Ez} , I_{Pz} , I_{Az} , and I_{Cz} are index sets of the latent neurons in the exteroceptive, proprioceptive, association, and executive areas, respectively. w_{ij} is the weight of the synaptic connection from the j th neuron to the i th neuron; $z_{t,j}^{(s)}$ is the output of j th latent (posterior) neuron at time step t ; τ is the time constant of the neuron; and b_i is the bias of the i th neuron. A deterministic neuron with a small time constant τ has a tendency to change its activity rapidly, while that with a large time constant has a tendency to change its activity slowly. We set the initial internal states of the deterministic neurons $h_{0,i}^{(s)}$ ($i \in I_{Ed}, I_{Pd}, I_{Ad}$) to 0 ($d_{0,i}^{(s)}$ is also 0).

The latent variable z in each area is assumed to follow a multivariate Gaussian distribution with a diagonal covariance matrix, meaning $z_{t,i}^{(s)}$ and $z_{t,j}^{(s)}$ are independent ($i, j \in I_{Ez}, I_{Pz}, I_{Az} \wedge i \neq j$). Here, the mean $\mu_{t,i}^{(s),p}$ and sigma (standard deviation) $\sigma_{t,i}^{(s),p}$ of the prior distribution $p(z_{t,i}^{(s)})$ in the exteroceptive, proprioceptive, and association areas are calculated from the previous deterministic state (prior experience) of the same area.

$$p(z_{t,i}^{(s)}) = p(z_{t,i}^{(s)} | d_{t-1,j}^{(s)}) = \mathcal{N}(z_{t,i}^{(s)}; \mu_{t,i}^{(s),p}, \sigma_{t,i}^{(s),p}). \quad (3)$$

$$\mu_{t,i}^{(s),p} = \tanh \left(\sum_j w_{ij} d_{t-1,j}^{(s)} \right), \quad (4)$$

$$\sigma_{t,i}^{(s),p} = \exp \left(\sum_j w_{ij} d_{t-1,j}^{(s)} \right). \quad (5)$$

Here, $(i \in I_{Ez} \wedge j \in I_{Ed}) \vee (i \in I_{Pz} \wedge j \in I_{Pd}) \vee (i \in I_{Az} \wedge j \in I_{Ad})$. The executive area has a prior distribution as $\mathcal{N}(0, 1)$ only at the initial step ($t = 1$) because it has a constant posterior state during sequential prediction generation, with the objective of assigning a specific executive-level posterior to each target sequence.

The posterior distribution in each area is calculated as,

$$q(z_{t,i}^{(s)} | e_{t:T^{(s)}}^{(s)}) = \begin{cases} q(z_{t-1,i}^{(s)} | e_{t-1:T^{(s)}}^{(s)}) = q(z_{1,i}^{(s)} | e_{1:T^{(s)}}^{(s)}) = \mathcal{N}(z_{1,i}^{(s)}; \mu_{1,i}^{(s),q}, \sigma_{1,i}^{(s),q}) & (i \in I_{Cz}), \\ \mathcal{N}(z_{t,i}^{(s)}; \mu_{t,i}^{(s),q}, \sigma_{t,i}^{(s),q}) & (i \in I_{Ez}, I_{Pz}, I_{Az}). \end{cases} \quad (6)$$

$$\mu_{t,i}^{(s),q} = \tanh(a_{t,i}^{(s),\mu}), \quad (7)$$

$$\sigma_{t,i}^{(s),q} = \exp(a_{t,i}^{(s),\sigma}), \quad (8)$$

$$z_{t,i}^{(s)} = \mu_{t,i}^{(s),q} + \sigma_{t,i}^{(s),q} \times \epsilon. \quad (9)$$

Here, $T^{(s)}$ represents the length of the s th target sequence. \mathbf{a} is the adaptive internal state of neurons representing posterior distributions and it is updated at each time step and for each target sequence during the learning process (or each time step through online inference). Adaptive variables \mathbf{a}_t are determined by prediction error signals $\mathbf{e}_{t:T}$ propagated by a back-propagation-through-time (BPTT) algorithm, meaning that the posterior of the latent state can be considered a prediction-error-related neural state. Adaptive variables \mathbf{a} are initialized by the corresponding initial internal states of the neurons representing prior distributions before the learning or inference process. Based on the posterior calculation, the latent state $z_{t,i}^{(s)}$ is obtained by sampling ϵ from $\mathcal{N}(0, 1)$.

Finally, predictions about exteroceptive and proprioceptive sensations are individually generated from exteroceptive and proprioceptive areas, respectively.

$$\hat{x}_{t,i}^{(s)} = \begin{cases} \tanh\left(\sum_{j \in I_{Ed}} w_{ij} d_{t,j}^{(s)}\right) & (i \in I_{Eo}), \\ \tanh\left(\sum_{j \in I_{Pd}} w_{ij} d_{t,j}^{(s)}\right) & (i \in I_{Po}). \end{cases} \quad (10)$$

Here, I_{Eo} and I_{Po} are index sets of output neurons for exteroceptive and proprioceptive predictions, respectively.

Parameter updates via free-energy minimization

The concept of FEP (5) derives from the fundamental fact that self-organizing biological agents must make their sensory states in a limited repertoire to remain alive (e.g., a human stays on the ground, not in the sea). Based on information theory, this notion can be formulated as suppression of the surprise (or the negative log-evidence) for sensations

\mathbf{x} over time. In the PV-RNN, the surprise over all time steps and target sequences can be written as:

$$\begin{aligned} \sum_{s \in I_S} & -\log p(\mathbf{x}_{1:T^{(s)}}^{(s)}) \\ &= \sum_{s \in I_S} \left[-\log \int p(\mathbf{x}_{1:T^{(s)}}^{(s)}, \mathbf{z}_{1:T^{(s)}}^{(s)}) d\mathbf{z}_{1:T^{(s)}}^{(s)} \right] \end{aligned} \quad (11)$$

$$= \sum_{s \in I_S} \left[-\log \int \prod_{t=1}^{T^{(s)}} [p(\mathbf{x}_t^{(s)} | \mathbf{d}_t^{(s)}) p(\mathbf{z}_t^{(s)} | \mathbf{d}_{t-1}^{(s)})] d\mathbf{z}_{1:T^{(s)}}^{(s)} \right]. \quad (12)$$

Here, I_S denotes the index set of target sequences. However, the surprise cannot be directly evaluated by the agent because it needs to know all the hidden states \mathbf{z} of the environment that cause sensations, as described on the right side of the equation (11). Here, FEP introduces a tractable quantity, free-energy, that bounds the surprise, and minimization of the surprise is replaced by minimization of the free-energy. The bound of the surprise in the PV-RNN can be derived by utilizing Jensen's inequality for a concave function f : $f(E[x]) \geq E[f(x)]$. For clarity, the summation over target sequences is temporarily omitted in the following equations. Then, equation (12) can be deformed as follows by introducing a dummy distribution for \mathbf{z}_1 , $q(\mathbf{z}_1)$.

$$\begin{aligned} & -\log p(\mathbf{x}_{1:T}) \\ &= -\log \int_{\mathbf{z}_1} d\mathbf{z}_1 q(\mathbf{z}_1) \int_{\mathbf{z}_{2:T}} d\mathbf{z}_{2:T} \frac{1}{q(\mathbf{z}_1)} \prod_{t=1}^T [p(\mathbf{x}_t | \mathbf{d}_t) p(\mathbf{z}_t | \mathbf{d}_{t-1})] \end{aligned} \quad (13)$$

$$\leq -\int_{\mathbf{z}_1} d\mathbf{z}_1 q(\mathbf{z}_1) \log \int_{\mathbf{z}_{2:T}} d\mathbf{z}_{2:T} \frac{1}{q(\mathbf{z}_1)} \prod_{t=1}^T [p(\mathbf{x}_t | \mathbf{d}_t) p(\mathbf{z}_t | \mathbf{d}_{t-1})]. \quad (14)$$

In equation (14), we use Jensen's inequality for a logarithmic function. The same procedure is done for $t = 2 : T$.

$$-\log p(\mathbf{x}_{1:T}) \leq -\int_{\mathbf{z}_1} d\mathbf{z}_1 q(\mathbf{z}_1) \cdots \int_{\mathbf{z}_T} d\mathbf{z}_T q(\mathbf{z}_T) \log \prod_{t=1}^T \left[\frac{p(\mathbf{x}_t | \mathbf{d}_t) p(\mathbf{z}_t | \mathbf{d}_{t-1})}{q(\mathbf{z}_t)} \right] \quad (15)$$

$$= -\int_{\mathbf{z}_1} d\mathbf{z}_1 q(\mathbf{z}_1) \cdots \int_{\mathbf{z}_T} d\mathbf{z}_T q(\mathbf{z}_T) \sum_{t=1}^T \left[\underbrace{\log p(\mathbf{x}_t | \mathbf{d}_t)}_A - \underbrace{\log \frac{q(\mathbf{z}_t)}{p(\mathbf{z}_t | \mathbf{d}_{t-1})}}_B \right]. \quad (16)$$

The first term in expression (16) is the expected negative log-likelihood under q given that \mathbf{d}_t depends on $\mathbf{z}_{1:t}$.

$$A = -\int_{\mathbf{z}_1} d\mathbf{z}_1 q(\mathbf{z}_1) \cdots \int_{\mathbf{z}_T} d\mathbf{z}_T q(\mathbf{z}_T) \sum_{t=1}^T \log p(\mathbf{x}_t | \mathbf{d}_t) \quad (17)$$

$$= -\sum_{t=1}^T E_{q(\mathbf{z}_{1:t})} [\log p(\mathbf{x}_t | \mathbf{d}_t)]. \quad (18)$$

In addition, the second term can be deformed into forms of Kullback-Leibler divergence (KLD) between $q(\mathbf{z}_t)$ and $p(\mathbf{z}_t|\mathbf{d}_{t-1})$ while being careful that \mathbf{d}_0 is independent from $\mathbf{z}_{1:T}$.

$$\begin{aligned} \text{B} &= \int_{\mathbf{z}_1} d\mathbf{z}_1 q(\mathbf{z}_1) \cdots \int_{\mathbf{z}_T} d\mathbf{z}_T q(\mathbf{z}_T) \sum_{t=1}^T \log \frac{q(\mathbf{z}_t)}{p(\mathbf{z}_t|\mathbf{d}_{t-1})} \end{aligned} \quad (19)$$

$$\begin{aligned} &= \int_{\mathbf{z}_1} d\mathbf{z}_1 q(\mathbf{z}_1) \log \frac{q(\mathbf{z}_1)}{p(\mathbf{z}_1|\mathbf{d}_0)} \\ &\quad + \int_{\mathbf{z}_1} d\mathbf{z}_1 q(\mathbf{z}_1) \cdots \int_{\mathbf{z}_T} d\mathbf{z}_T q(\mathbf{z}_T) \sum_{t=2}^T \log \frac{q(\mathbf{z}_t)}{p(\mathbf{z}_t|\mathbf{d}_{t-1})} \end{aligned} \quad (20)$$

$$= D_{KL}[q(\mathbf{z}_1)||p(\mathbf{z}_1|\mathbf{d}_0)] + \sum_{t=2}^T E_{q(\mathbf{z}_{1:t-1})} [D_{KL}[q(\mathbf{z}_t)||p(\mathbf{z}_t|\mathbf{d}_{t-1})]] \quad (21)$$

A dummy distribution $q(\mathbf{z}_t)$ can be replaced by the posterior distribution determined by the back-propagated prediction error $q(\mathbf{z}_t|\mathbf{e}_{t:T})$. Thus, using equations (18) and (21), the bound of the surprise can be written as,

$$\begin{aligned} -\log p(\mathbf{x}_{1:T}) &\leq -\sum_{t=1}^T E_{q(\mathbf{z}_{1:t}|\mathbf{e}_{t:T})} [\log p(\mathbf{x}_t|\mathbf{d}_t)] + D_{KL}[q(\mathbf{z}_1|\mathbf{e}_{1:T})||p(\mathbf{z}_1|\mathbf{d}_0)] + \\ &\quad \sum_{t=2}^T E_{q(\mathbf{z}_{1:t-1}|\mathbf{e}_{t-1:T})} [D_{KL}[q(\mathbf{z}_t|\mathbf{e}_{t:T})||p(\mathbf{z}_t|\mathbf{d}_{t-1})]] \end{aligned} \quad (22)$$

In the experiment, we resolve calculation of the expectations of negative log-likelihood and KLD under q by considering single sampling to reduce computational costs.

$$-\log p(\mathbf{x}_{1:T}) \leq \sum_{t=1}^T (-\log p(\mathbf{x}_t|\mathbf{d}_t) + D_{KL}[q(\mathbf{z}_t|\mathbf{e}_{t:T})||p(\mathbf{z}_t|\mathbf{d}_{t-1})]) \quad (23)$$

Eventually, by introducing the meta-prior and considering the summation over different target sequences, the free-energy F (the bound of the surprise) in the PV-RNN is formulated as:

$$F = \sum_{s \in I_S} \sum_{t=1}^{T^{(s)}} F_t^{(s)} \quad (24)$$

$$\begin{aligned} F_t^{(s)} &= \underbrace{-\log p(\mathbf{x}_t^{(s)}|\mathbf{d}_t^{(s)})}_{\text{Accuracy}} \\ &\quad + \sum_{l=1}^3 W^{(l)} \underbrace{\left(D_{KL}[q(\mathbf{z}_t^{(l),(s)}|\mathbf{e}_{t:T}^{(s)})||p(\mathbf{z}_t^{(l),(s)}|\mathbf{d}_{t-1}^{(l),(s)})] \right)}_{\text{Complexity}} \end{aligned} \quad (25)$$

Here, $W^{(l)}$ denotes the meta-prior at l th network level. The first term in expression (25) (negative accuracy term) is the negative log-likelihood. For simplicity, we assume that each sensory state follows a Gaussian distribution with unit variance. Then, the first term becomes just the prediction error between the real $x_t^{(s)}$ and predicted $\hat{x}_t^{(s)}$ sensations (plus a constant term, omitted here).

$$-\text{Accuracy} = \sum_{i \in I_{\text{Eo}} \cup I_{\text{Po}}} \frac{1}{2} \left(x_{t,i}^{(s)} - \hat{x}_{t,i}^{(s)} \right)^2. \quad (26)$$

This assumption sets the precision of the prediction error to a constant value and makes it easy to consider the relative precision of prior beliefs compared to prediction error. In the experiment, we divided the accuracy term by the dimension of each exteroceptive and proprioceptive sensation.

On the other hand, the second term (complexity term) is the KLD between the posterior and prior distributions of the latent variables. Note that variables of the posterior are updated through both the accuracy and complexity terms, but those of the prior are updated only through the complexity term. Therefore, the complexity term represents only the influence of prior beliefs, which is controlled by the meta-prior W . Under the assumption that the prior and posterior distributions follow a multivariate Gaussian distribution with a diagonal covariance matrix, as described above, the KLD is computed analytically as (17, 18),

$$\text{Complexity} = \sum_i \left(\log \frac{\sigma_{t,i}^{(s),p}}{\sigma_{t,i}^{(s),q}} + \frac{(\mu_{t,i}^{(s),p} - \mu_{t,i}^{(s),q})^2 + (\sigma_{t,i}^{(s),q})^2}{2(\sigma_{t,i}^{(s),p})^2} - \frac{1}{2} \right). \quad (27)$$

Here, $i \in I_{\text{Ez}} \cup I_{\text{Pz}}$ (if $l = 1$), $i \in I_{\text{Az}}$ (if $l = 2$), and $i \in I_{\text{Cz}}$ (if $l = 3$). In the experiment, we divided the complexity term by the dimension of latent variables for each area. Note that if $l = 3$ (executive area), the complexity term exists at only $t = 1$, although we write the equation in a general way for simplicity.

In the learning phase (Extended Data Fig. 1), synaptic weights w and adaptive variables a are updated to minimize the free-energy over all time steps and target sequences as,

$$F = \sum_{s \in I_{\text{S}}} \sum_{t=1}^{T^{(s)}} F_t^{(s)}. \quad (28)$$

In the test phase after learning (Extended Data Fig. 2), only adaptive variables a are updated, while synaptic weights are fixed. In this phase, the free-energy within a short time window H is summed as

$$F = \sum_{t'=t-H+1}^t F_{t'}. \quad (29)$$

Using the summed free-energy, adaptive variables $a_{t-H+1:t}$ within the time window of all areas are updated, whereas the time window slides as the network time step t is incremented.

In both learning and test phases, we used the Adam optimizer (37) for parameter updates, where the partial derivative of the free-energy with respect to each parameter is calculated by the BPTT algorithm.

Experimental environment

We set a 3-axis robotic arm in a simulated square space $[-1, 1] \times [-1, 1]$. The lengths of the robot’s links are 0.1, 0.3, and 0.5. Each joint angle was limited to range from 0 to π [rad] and normalized to range from -0.8 to 0.8 to match the range of the neural network output. In addition, the PV-RNN receives the 2-dimensional position of a red object as an exteroceptive sensation. During task execution, the robot receives the 5-dimensional sensations every 250 ms.

Learning

The PV-RNN learned to reproduce target sensorimotor sequences prepared in advance. First, we recorded 24 sequences of joint angles while the experimenter manually manipulated the left arm of a physical robot (Rakuda, developed by Robotis). For each sequence, the experimenter performed 10 repetitions generating a random movement and returning to the set posture within five seconds (20 time steps). Therefore, the length of each sequence is 200 time steps. We used joint angles from left shoulder pitch, left shoulder roll, and the left elbow of Rakuda as 3-dimensional proprioception data of the simulated robot arm. Next, we prepared exteroception data for a self-produced condition by setting the object position as the hand position of the simulated arm robot that was calculated by the forward kinematics using the recorded joint angle data. In this way, we obtained 24 target sequences for self-produced conditions in which exteroceptive and proprioceptive sensations are correlated. Finally, we prepared target sequences for externally produced conditions by shuffling the combination of exteroceptive and proprioceptive sequences. By doing this, we obtained 24 target sequences for externally produced conditions in which exteroceptive and proprioceptive sensations are not correlated. This shuffling procedure ensures that the total numbers of changes in sensations are the same for self-produced and externally produced conditions in the learning phase. The PV-RNN learned to reproduce the prepared 48 training datasets via free-energy minimization.

Online inference

We prepared an additional 8 exteroceptive sequences as test data that were used in externally produced conditions in the test phase. Before a test trial, the initial states of adaptive variables \mathbf{a}_1 in all areas were set to the median values obtained for 24 training datasets of the self-produced condition developed through learning. Based on the initial posterior states corresponding to self-produced condition, the robot first moved the object by itself during time steps 0-100. The robot controlled its joint angles via active inference using the PID controller, for which proprioceptive predictions were used as target joint angles. Then, during time steps 100-200, the environmental condition was shifted to the externally produced condition, although the robot kept generating spontaneous behaviors by itself via active inference. In the externally produced condition, the object position was set from test data. The goal of the robot was to flexibly recognize the environmental change by updating adaptive variables via free-energy minimization. The online inference process was performed based

on an interaction between top-down prediction generation and bottom-up posterior updates. In the top-down prediction generation process, the PV-RNN generated sensory predictions $\hat{x}_{t-H+1:t}$ corresponding to time steps from $t - H + 1$ to t , based on the posterior of latent states $z_{t-H+1:t}$. In the bottom-up modulation process, the free-energy at each time step within time window H was calculated using prediction errors for exteroception and proprioception, for which target sensations were the real object position and joint angles from $t - H + 1$ to t . Adaptive variables $a_{t-H+1:t}$ within the time window were updated to minimize the free-energy summed over time steps, and sensory predictions within the time window were re-generated using the updated posterior states. By repeating top-down prediction generation and bottom-up posterior updates for a certain duration, the PV-RNN generated the prior of latent states for time step $t + 1$. The generated prior was used to initialize the posterior for time step $t + 1$, and predictions about sensations for time step $t + 1$ were generated from the posterior. Using proprioceptive predictions for time step $t + 1$ as the target joint angles, the robot moved the joint angles using the PID controller. At the same time, the robot received exteroceptive sensations at time step $t + 1$. After that, the robot's time step was incremented and the online inference process was performed for the newly received sensations. This inference process, in which the recognition and prediction in the past are reconstructed from current sensations, corresponds to a "postdiction" process.

Parameter settings

The dimension of latent variables z in the exteroceptive and proprioceptive areas was 1, and that in the association area was 3. Therefore, the total dimension of latent neurons in sensory and association areas was the same as the sensory dimension. The dimension of latent variables in executive area was 1. A preliminary experiment showed that a smaller number of latent neurons in the association area led to a lower level of sensory attenuation, supporting the idea that sensory attenuation is a consequence of representing sensorimotor correlation in the association area (Extended Data Fig. 4a). In addition, we confirmed that no executive-level latent state resulted in a highly decreased level of sensory attenuation, suggesting an important role of the executive-level latent state (Extended Data Fig. 4b). The numbers of deterministic neurons in the exteroceptive, proprioceptive, and association areas were all 15. In a preliminary experiment, we evaluated development of sensory attenuation for settings of 10, 15, or 20 deterministic neurons and confirmed that the setting of 15 neurons showed the largest sensory attenuation (Extended Data Fig. 10a). We set the time constant τ to half the number of deterministic neurons (8 neurons) to 2 and that of the other neurons (7 neurons) to 4, as the simplest multiple timescale setting. We set the same multiple timescale property for both the sensory and association areas. This is because we thought that the PV-RNN controlled which levels of the network hierarchy should be used to represent sensations, depending on the condition. Actually, the experimental results show that the PV-RNN mainly used the association area in the self-produced condition and both the sensory and association areas in an externally produced condition, in which the timescale property included in sensations was the same for the two conditions. In a preliminary experiment, we confirmed that the multiple timescale setting led to greater sensory attenuation compared to the single timescale setting $\tau = 2$ for all deterministic

neurons (Extended Data Fig. 10b). Synaptic weights were initialized with random values that follow Gaussian distributions $N(0, \frac{2}{n_{in}})$, where n_{in} is the number of inputs to a neuron. Biases of deterministic neurons were initialized with and fixed to random values following a Gaussian distribution $N(0, 10)$, for which the variance of biases is close to the firing threshold variability found in biological neurons (38), as well as the optimal value in a spiking neural network model (39) and a recurrent neural network model (34). We trained 10 networks with different initial synaptic weights for each hyper-parameter setting for quantitative evaluations. In the learning phase, parameters including synaptic weights w and adaptive variables a were updated 200,000 times with the Adam optimizer. We used the same parameter setting of Adam as in the original paper: $\alpha = 0.001$ (learning rate), $\beta_1 = 0.9$, and $\beta_2 = 0.999$. In the test phase, adaptive variables a were updated 50 times at each time step for a time window of length $H = 10$ with $\alpha = 0.09$. We chose the optimal parameter setting in the test phase from the combinations of $\alpha = \{0.001, 0.005, 0.01, 0.03, 0.05, 0.07, 0.09, 0.1, 0.2, 0.3, 0.4, 0.5\} \times H = \{10, 15\}$ by evaluating levels of prediction error in the baseline meta-prior setting.

Statistical analysis

We used paired t-tests for statistical analyses of network behaviors in the baseline model, such as the posterior response and the level of the prior sigma. In statistical analyses of the effects of meta-prior settings, we used one-way ANOVA followed by Dunnett’s test. All statistical tests were two-tailed, and the significance level was set at $p < 0.05$. No statistical methods were used to determine sample sizes in advance. Data analyses were conducted using R software (version 3.3.2).

Supplementary Result and Discussion

Development of psychiatric disorders with shifts in the meta-prior

After confirming the development of sensory attenuation in the baseline model ($W^{(1)} = W^{(2)} = W^{(3)} = 0.005$), we investigated effects of shifts in the meta-prior at each network level. Extended Data Fig. 5a shows a test result for a small association-level meta-prior ($W^{(2)} = 0.001$, $W^{(1)} = W^{(3)} = 0.005$) (Supplementary Video 2), where the posterior in the association area is highly sensitive to prediction errors and ignores the prior. In this case, the association-level latent mean $\mu^{(2)}$ fluctuates greatly with reduced periodicity, although modulation of the sensory-level latent mean $\mu^{(1)}$ was small in self-produced conditions such as the baseline model. The sensitive latent response in the association area reflected a stronger tendency to adjust the posterior in the association area to minimize prediction errors, compared to the normal case. This sometimes led to difficulty in switching the executive-level latent state $\mu^{(3)}$ (and the sensory-level latent response) in the face of the environmental change, suggesting a reciprocal reduction of prediction-error flow into the executive area (Extended Data Fig. 5b).

Extended Data Fig. 5c shows a case of a large association-level meta-prior ($W^{(2)} = 0.025$, $W^{(1)} = W^{(3)} = 0.005$) (Supplementary Video 3), in which prediction errors tend to be reduced more by adjusting the posterior in sensory areas than in the association area. The sensory-level latent response in the self-produced condition seemed to be large, as with the externally produced condition, indicating a failure of sensory attenuation. In addition, the recurrent network experienced large prediction errors, even in the self-produced condition, leading to inappropriate switching of the executive-level latent state and mismatches between the real and recognized environmental condition. This suggests that prediction errors that could not be resolved by sensory areas flowed into the executive area because of an intrinsically strong prior in the association area (Extended Data Fig. 5d).

We quantitatively analyzed network behaviors, varying the association-level meta-prior ($W^{(2)} = 0.001, 0.0025, 0.005, 0.01, 0.025$). Extended Data Fig. 6a-b show the changes in levels of prediction errors in the self-produced and the externally produced conditions in the test phase, respectively. We observed different effects induced by small and large association-level meta-priors. Specifically, compared to baseline settings, small association-level meta-priors resulted in large prediction errors in both self-produced and externally produced conditions, while large association-level meta-priors led to large prediction errors, particularly in the self-produced condition. One-way analysis of variance (ANOVA) revealed significant differences among the five meta-prior settings in prediction errors in both self-produced ($F(4, 45) = 7.45, p < 0.001$) and externally produced conditions ($F(4, 45) = 5.16, p = 0.0017$). Post hoc multiple comparisons reported that levels of prediction errors in the self-produced condition were significantly larger in $W^{(2)} = 0.001$ ($p < 0.001$) and $W^{(2)} = 0.025$ ($p = 0.0015$), compared to $W^{(2)} = 0.005$ (p values were corrected based on the Dunnett's test). In addition, the post hoc Dunnett's test indicated that the level of prediction errors in

externally produced conditions was significantly larger in $W^{(2)} = 0.001$ than $W^{(2)} = 0.005$ ($p = 0.0057$). An additional analysis revealed reduced prediction errors for training data in small association-level meta-prior settings (Extended Data Fig. 7a-b), suggesting overfitting to training data and reduced generalization.

Extended Data Fig. 6c shows attenuation of the sensory-level posterior response in the test phase. The attenuation level is calculated by subtracting the posterior response in the self-produced condition from that in the externally produced condition. The average attenuation level was reduced by a small or large association-level meta-prior, reflecting the difficulty of recognizing an environmental change or a deficit in attenuating the sensory-level posterior response in self-produced condition. One-way ANOVA indicated a significant difference in attenuation level among the five settings ($F(4, 45) = 2.9, p = 0.032$). The post hoc Dunnett's test reported that the attenuation level in $W^{(2)} = 0.025$ was significantly lower than that in $W^{(2)} = 0.005$ (baseline) ($p = 0.044$), but a significant difference between $W^{(2)} = 0.001$ and $W^{(2)} = 0.005$ was not found ($p = 0.11$). This indicates that a large association-level meta-prior had a chronic influence on modulation of neural responses in sensory areas.

We investigated whether reduced sensory attenuation in the test phase was induced by difficulty in recognizing an environmental change or a deficit in development of sensory attenuation itself. Extended Data Fig. 6d-g show the effect of small or large association-level meta-priors on development of sensory attenuation through learning. In the case of a small association-level meta-prior ($W^{(2)} = 0.001$), a sensory-level posterior response and prior sigma normally became lower in the self-produced condition compared to the externally produced condition during the learning process (Extended Data Fig. 6d-e and 7c). On the other hand, a large association-level meta-prior ($W^{(2)} = 0.025$) induced a deficit in attenuating sensory-level posterior responses and prior sigma through learning (Extended Data Fig. 6f-g and 7c). Overall, small association-level meta-priors reduced generalization with normal development of sensory attenuation, while large association-level meta-priors reduced the distinction between self-produced and externally produced conditions.

We also investigated effects induced by shifts in sensory-level or executive-level meta-priors (Extended Data Fig. 8-9). These had no significant impacts on behavioral performance (measured as the level of prediction error) in the test phase, although small and large sensory-level meta-priors induced alterations in sensory attenuation.

Implications for computational mechanisms of psychiatric disorders

Sets of unusual behaviors were induced by shifts in the meta-prior, a hyper-parameter determining the intrinsic strength of the prior compared to the prediction error at each network level. In the basic Bayesian model, the practitioner must manually set the prior, including its precision, for computing the posterior. However, in our model, the prior in each network area is epigenetically self-organized through learning, with an influence of the higher meta-level parameter (i.e., the meta-prior). We assumed that the meta-prior is an innate characteristic determining developmental features of the prior and prediction-error flow in the biological brain, although its neural substrate remains unspecified. In our experiment, a large meta-prior in the association area led to reduced sensory attenuation (i.e., a weak prior in sensory areas). The network setting also induced large

prediction errors, even for self-produced sensations, leading to inappropriate switching of higher-level belief about the cause of sensation. The false inference that “I” was not the agent generating sensations (or the opposite) could result in disturbance of the sense of agency. These impairments in self-other distinction may be associated with core symptoms of schizophrenia, such as delusions and hallucinations (3, 4). This explanation may resolve conflicting evidence for a strong or weak prior in schizophrenia (4, 27, 28). On the other hand, a small meta-prior in the association area led to reduced generalization and a certain level of difficulty, albeit statistically non-significant, in switching higher-level belief. These characteristics may be analogous to characteristics of ASD (30), such as difficulty in turn-taking with other people or resistance to change. In the network setting, sensory attenuation developed normally through learning, although the failure of executive control led to an apparent reduction of sensory attenuation in the test phase. That is, sensory attenuation normally occurred if the environmental condition was appropriately recognized by the neural network. This may be consistent with previous studies showing that individuals with ASD exhibit normal sensory attenuation in situations in which an environmental condition was explicitly informed prior to an experiment (29, 32). Our explanation connects the observation of normal sensory attenuation and a weak prior hypothesis for ASD (30, 31). Our results suggest a potential mechanistic difference between characteristics of schizophrenia and ASD.

References

1. L. Weiskrantz, J. Elliot, and C. Darlington. Preliminary observations on tickling oneself. *Nature*, 230(5296):598–599, Apr 1971.
2. Daniel M. Wolpert, Zoubin Ghahramani, and Michael I. Jordan. An internal model for sensorimotor integration. *Science*, 269(5232):1880–1882, Sep 1995.
3. Sarah-Jayne Blakemore, Daniel Wolpert, and Chris Frith. Why can’t you tickle yourself? *NeuroReport*, 11(11):R11–R16, 2000.
4. Harriet Brown, Rick A. Adams, Isabel Parees, Mark Edwards, and Karl Friston. Active inference, sensory attenuation and illusions. *Cognitive Processing*, 14(4):411–427, Nov 2013.
5. Karl Friston. The free-energy principle: a unified brain theory? *Nature Reviews Neuroscience*, 11(2):127–138, Feb 2010.
6. Andy Clark. Whatever next? predictive brains, situated agents, and the future of cognitive science. *Behavioral and Brain Sciences*, 36(3):181–204, 2013.
7. Niclas Braun, Stefan Debener, Nadine Spychala, Edith Bongartz, Peter Sörös, Helge H. O. Müller, and Alexandra Philipsen. The senses of agency and ownership: A review. *Frontiers in Psychology*, 9:535, Apr 2018.
8. Roberto Legaspi and Taro Toyoizumi. A bayesian psychophysics model of sense of agency. *Nature Communications*, 10(1):4250, Sep 2019.
9. John A. Dewey and Günther Knoblich. Do implicit and explicit measures of the sense of agency measure the same thing? *PLOS ONE*, 9(10):e110118, Oct 2014.
10. Sarah-J. Blakemore, Daniel M. Wolpert, and Chris D. Frith. Central cancellation of self-produced tickle sensation. *Nature Neuroscience*, 1(7):635–640, Nov 1998.
11. Pamela Bäß, Thomas Jacobsen, and Erich Schröger. Suppression of the auditory n1 event-related potential component with unpredictable self-initiated tones: Evidence for internal forward models with dynamic stimulation. *International Journal of Psychophysiology*, 70(2):137–143, Nov 2008.
12. B. Ezgi Arikan, Bianca M. van Kemenade, Kornelius Podranski, Olaf Steinsträter, Benjamin Straube, and Tilo Kircher. Perceiving your hand moving: Bold suppression in sensory cortices and the role of the cerebellum in the detection of feedback delays. *Journal of Vision*, 19(14)(4), Dec 2019.
13. Paul M. Bays, Daniel M. Wolpert, and J. Randall Flanagan. Perception of the consequences of self-action is temporally tuned and event driven. *Current Biology*, 15(12):1125–1128, Jun 2005.
14. Konstantina Kilteni, Benjamin Jan Andersson, Christian Houborg, and H. Henrik Ehrsson. Motor imagery involves predicting the sensory consequences of the imagined movement. *Nature Communications*, 9(1617):1–9, Apr 2018.

15. Noham Wolpe, James N. Ingram, Kamen A. Tsvetanov, Linda Geerligs, Rogier A. Kievit, Richard N. Henson, Daniel M. Wolpert, Lorraine K. Tyler, Carol Brayne, Edward Bullmore, and et al. Ageing increases reliance on sensorimotor prediction through structural and functional differences in frontostriatal circuits. *Nature Communications*, 7(1):13034, Oct 2016.
16. Rick A. Adams, Stewart Shipp, and Karl J. Friston. Predictions not commands: active inference in the motor system. *Brain Structure and Function*, 218(3):611–643, May 2013.
17. Ahmadreza Ahmadi and Jun Tani. A novel predictive-coding-inspired variational rnn model for online prediction and recognition. *Neural Computation*, 31(11):2025–2074, Nov 2019.
18. Wataru Ohata and Jun Tani. Investigation of the sense of agency in social cognition, based on frameworks of predictive coding and active inference: A simulation study on multimodal imitative interaction. *Frontiers in Neurorobotics*, 14:61, Sep 2020.
19. Katsuma Inoue, Kohei Nakajima, and Yasuo Kuniyoshi. Designing spontaneous behavioral switching via chaotic itinerancy. *Science Advances*, 6(46):eabb3989, Nov 2020.
20. Patrick Haggard and Ben Whitford. Supplementary motor area provides an efferent signal for sensory suppression. *Cognitive Brain Research*, 19(1):52–58, Mar 2004.
21. Rebecca Boehme, Steven Hauser, Gregory J. Gerling, Markus Heilig, and Håkan Olausson. Distinction of self-produced touch and social touch at cortical and spinal cord levels. *Proceedings of the National Academy of Sciences*, 116(6):2290, Feb 2019.
22. David M. Eagleman. The where and when of intention. *Science*, 303(5661):1144–1146, Feb 2004.
23. E. Charles Leek and Stephen J. Johnston. Functional specialization in the supplementary motor complex. *Nature Reviews Neuroscience*, 10(1):78–78, Jan 2009.
24. Angela J. Yu and Peter Dayan. Uncertainty, neuromodulation, and attention. *Neuron*, 46(4):681–692, May 2005.
25. Laura K. Pynn and Joseph F.X. DeSouza. The function of efference copy signals: Implications for symptoms of schizophrenia. *Vision Research*, 76:124–133, Jan 2013.
26. Konstantina Kilteni, Christian Houborg, and H Henrik Ehrsson. Rapid learning and unlearning of predicted sensory delays in self-generated touch. *eLife*, 8:e42888, Nov 2019.
27. A. R. Powers, C. Mathys, and P. R. Corlett. Pavlovian conditioning–induced hallucinations result from overweighting of perceptual priors. *Science*, 357(6351):596–600, Aug 2017.

28. Philip R. Corlett, Guillermo Horga, Paul C. Fletcher, Ben Alderson-Day, Katharina Schmack, and Albert R. Powers. Hallucinations and strong priors. *Trends in Cognitive Sciences*, 23(2):114–127, Feb 2019.
29. Sarah-Jayne Blakemore, Teresa Tavassoli, Susana Calò, Richard M. Thomas, Caroline Catmur, Uta Frith, and Patrick Haggard. Tactile sensitivity in asperger syndrome. *Brain and Cognition*, 61(1):5–13, Jun 2006.
30. Helene Haker, Maya Schneebeli, and Klaas Enno Stephan. Can bayesian theories of autism spectrum disorder help improve clinical practice? *Frontiers in Psychiatry*, 7, Jun 2016.
31. Colin J. Palmer, Rebecca P. Lawson, and Jakob Hohwy. Bayesian approaches to autism: Towards volatility, action, and behavior. *Psychological Bulletin*, 143(5):521–542, 2017.
32. Johanna J.S. Finnemann, Kate Plaisted-Grant, James Moore, Christoph Teufel, and Paul C. Fletcher. Low-level, prediction-based sensory and motor processes are unimpaired in autism. *Neuropsychologia*, 156:107835, Jun 2021.
33. Yuichi Yamashita and Jun Tani. Emergence of functional hierarchy in a multiple timescale neural network model: A humanoid robot experiment. *PLoS Comput. Biol.*, 4(11):e1000220, nov 2008.
34. Hayato Idei, Shingo Murata, Yuichi Yamashita, and Tetsuya Ogata. Homogeneous intrinsic neuronal excitability induces overfitting to sensory noise: A robot model of neurodevelopmental disorder. *Frontiers in Psychiatry*, 11:762, Aug 2020.
35. Arseny Finkelstein, Lorenzo Fontolan, Michael N. Economo, Nuo Li, Sandro Romani, and Karel Svoboda. Attractor dynamics gate cortical information flow during decision-making. *Nature Neuroscience*, 24(6):843–850, Jun 2021.
36. K. Newell, Y. Liu, and G. Mayer-Kress. Time scales in motor learning and development. *Psychological review*, 108 1:57–82, 2001.
37. Diederik P. Kingma and Jimmy Ba. Adam: A method for stochastic optimization, 2017.
38. Rony Azouz and Charles M. Gray. Dynamic spike threshold reveals a mechanism for synaptic coincidence detection in cortical neurons *in vivo*. *Proceedings of the National Academy of Sciences*, 97(14):8110–8115, Jul 2000.
39. J. F. Mejias and A. Longtin. Optimal heterogeneity for coding in spiking neural networks. *Physical Review Letters*, 108(22):228102–1–5, May 2012.

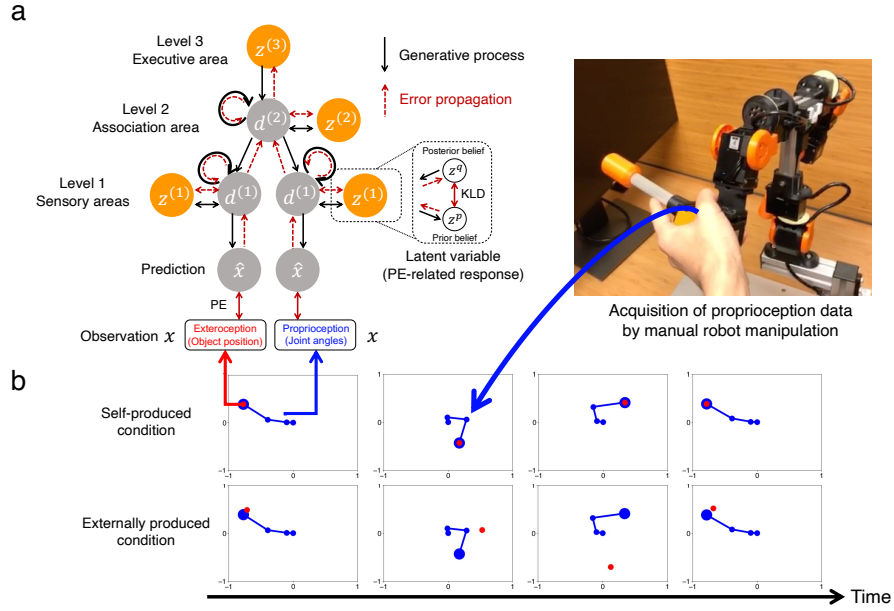


Figure 1: Training setting. **(a)** Hierarchical recurrent network updating of synaptic weights and posterior beliefs in all areas via minimization of free-energy determined by the prediction error (PE) and Kullback-Leibler divergence (KLD) between the posterior and the prior. **(b)** Spontaneous sensorimotor patterns learned by the recurrent network.

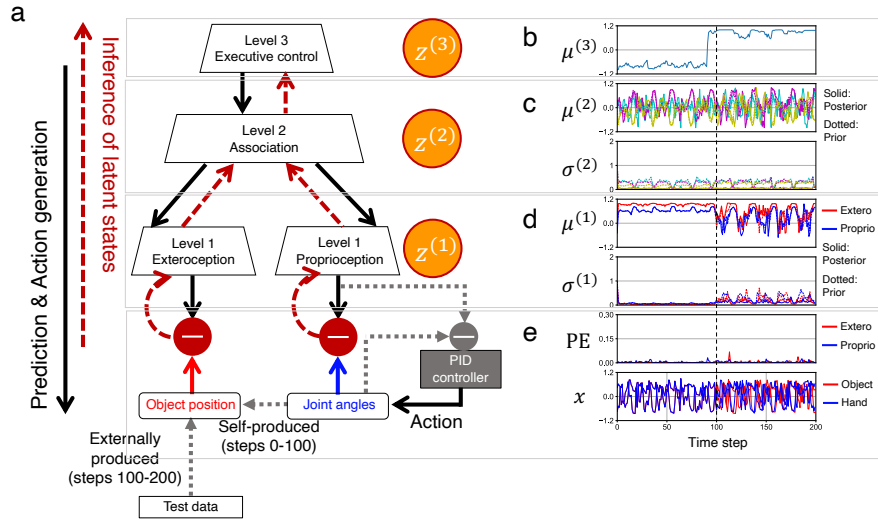


Figure 2: Test setting and an example of the result. **(a)** Online inference of latent states and action generation by a PID controller, with synaptic weights fixed. **(b)** Executive-level posterior mean. **(c)** Association-level posterior and prior distributions. **(d)** Sensory-level posterior and prior distributions in exteroceptive and proprioceptive areas. **(e)** Prediction error (PE) and real sensations for exteroception and proprioception. For clarity, proprioception is represented as the 2-dimensional hand position, although the actual proprioception comprises 3-dimensional joint angles.

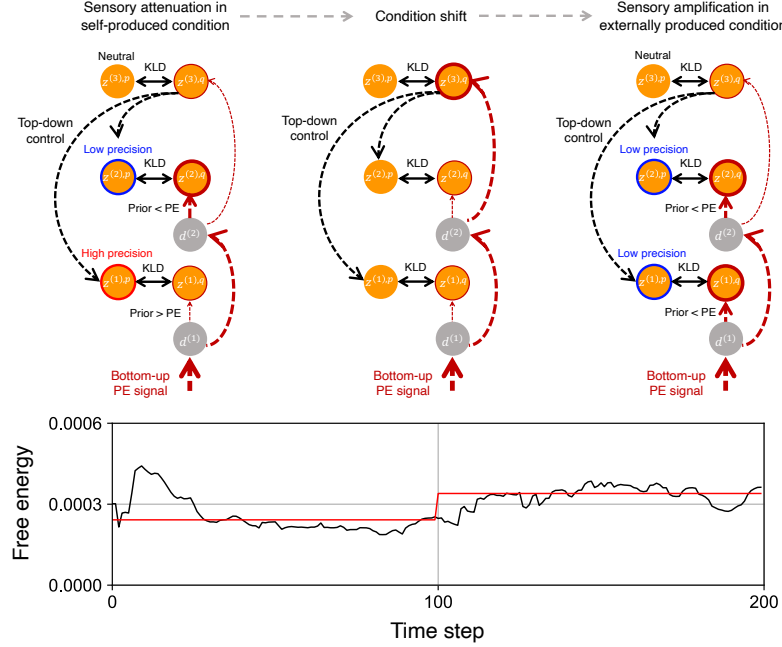


Figure 3: The self-organized mechanism for the transition between sensory attenuation in self-produced conditions and sensory amplification in externally produced conditions. For each sensorimotor condition, a particular global free-energy minimum in the network was developed through learning, which was characterized by the corresponding top-down precision control and bottom-up prediction-error (PE) flow. Consequently, in self-produced conditions, the recurrent network mainly adjusted only the posterior in the association area $z^{(2),q}$ to minimize prediction errors by increasing precision of priors in sensory areas $z^{(1),p}$ and decreasing precision of prior in the association area $z^{(2),p}$. On the other hand, in externally produced conditions, it adjusted posteriors in both sensory and association areas ($z^{(1),q}$ and $z^{(2),q}$) by decreasing precision of priors in both sensory and association areas. The shift of the sensorimotor condition triggered modulation of the posterior in the executive area $z^{(3),q}$ as well as the transition from one free-energy state to another in the network (bottom timeseries). This induced a qualitative change in the network behavior and a shift between attenuating and amplifying responses in the sensory areas. The black line in the timeseries of the free-energy describes the 20-step moving average (values within the first 19 steps are calculated as averages from the initial to the current step). The red line is the average over the first 100 steps (i.e., self-produced condition) or the last 100 steps (i.e., externally produced condition). The values are averages over 80 test trials performed by 10 different networks.

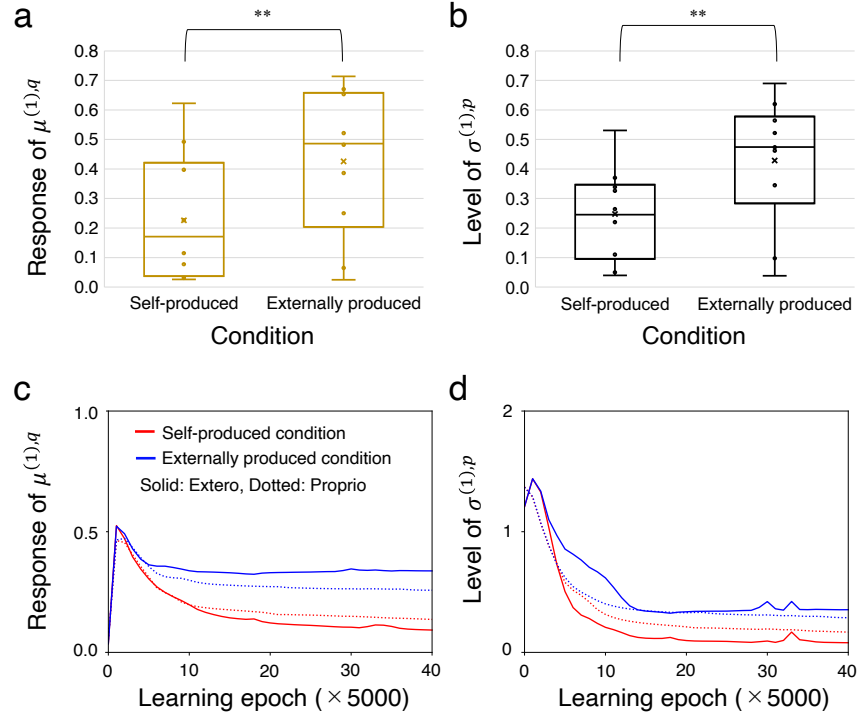
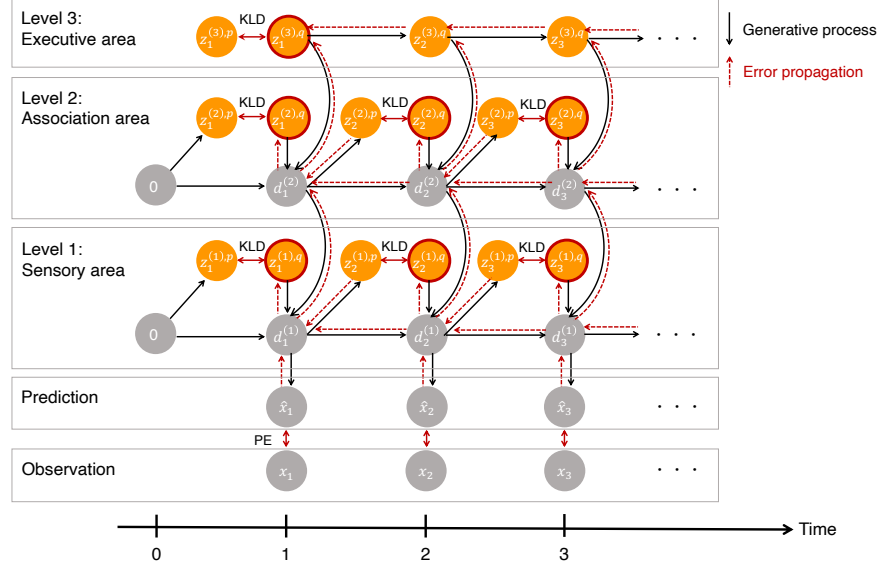
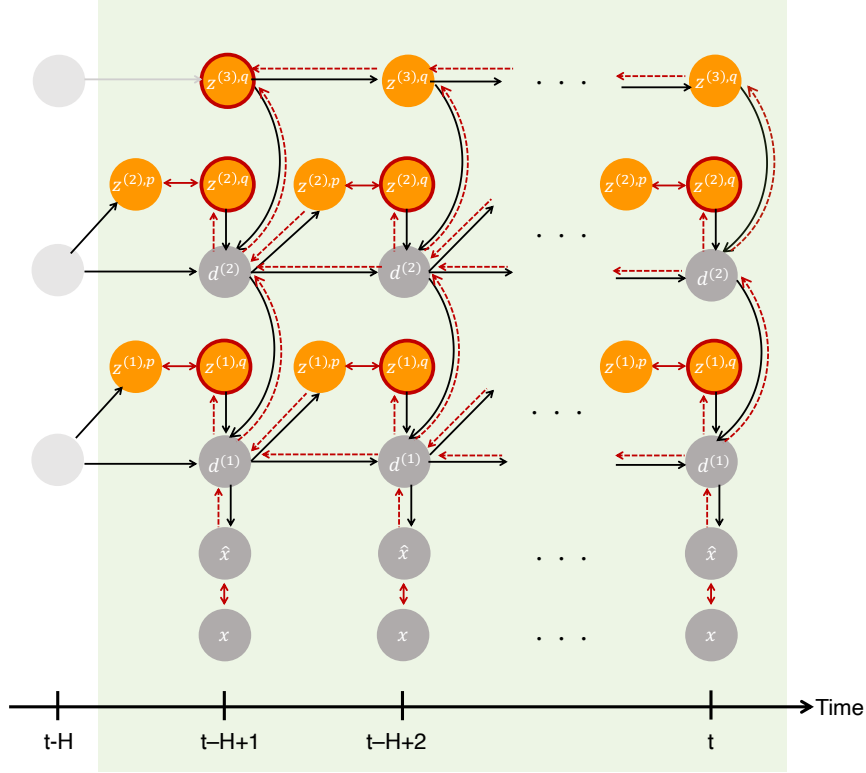


Figure 4: Sensory-level neural response in the test phase and its development in the learning phase. **(a)** Box-and-whiskers plots showing the difference in sensory-level posterior response between self-produced and externally produced conditions. **(b)** Box-and-whiskers plots showing the difference in the sensory-level prior sigma between the two conditions. In (a) and (b), each plot is an average of 100 time steps, 2 sensory areas, and 8 test trials by each of 10 trained networks (center line, median; cross, mean; box limits, upper and lower quartiles; whiskers, 1.5x interquartile range). $**p < 0.01$. **(c)** Development of the posterior response for the two conditions in the exteroceptive and proprioceptive areas. **(d)** Development of sensory-level prior sigma. In (c) and (d), the value is averaged over 200 time steps, 24 training datasets, and 10 different networks in each learning epoch.

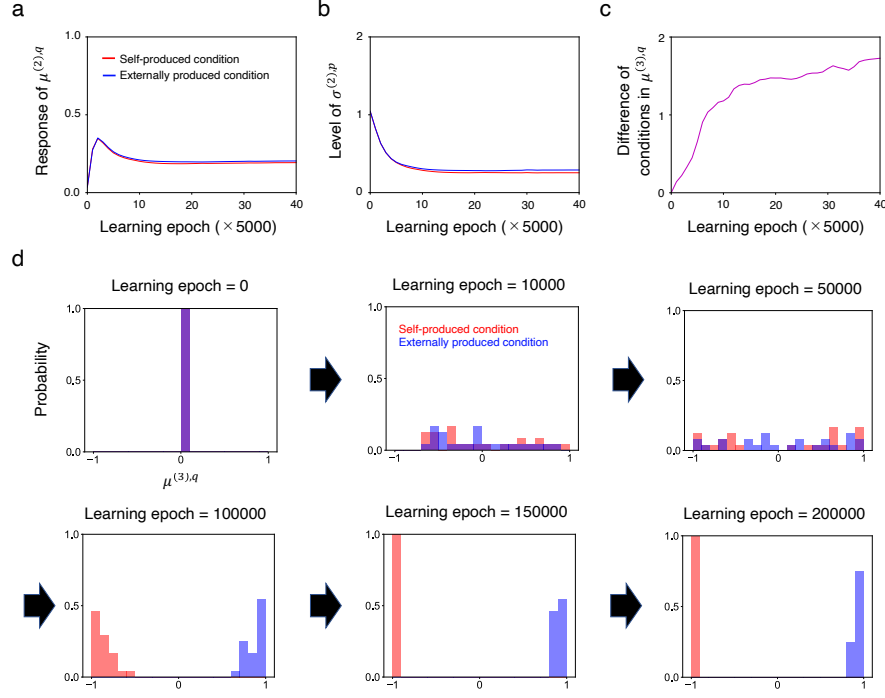
Extended Data:



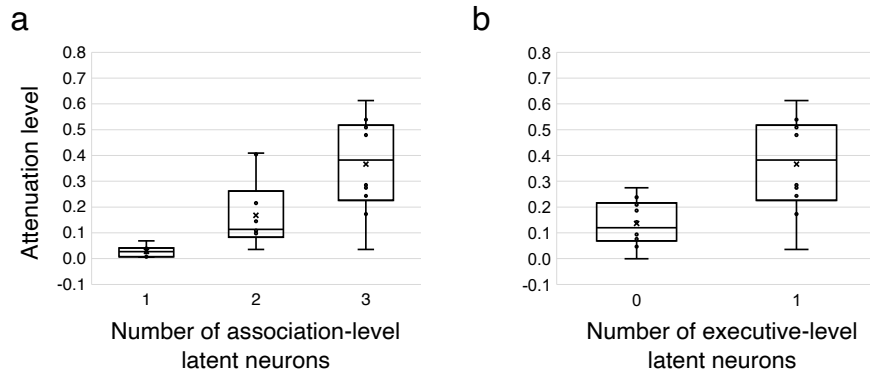
Extended Data Figure 1: Temporal processing of the recurrent neural network. In the learning phase, the recurrent network updates the posteriors of latent variables in all areas ($z_{1:T}^{(1),q}$, $z_{1:T}^{(2),q}$, and $z_{1:T}^{(3),q}$) and time-constant synaptic weights via minimization of free-energy over the time length (T) of training data. Initial deterministic states d_0 in all areas are set to 0. The initial prior distribution z_1^p in the executive area is set to a unit Gaussian distribution $\mathcal{N}(0, 1)$. For simplicity, the distributed structure of sensory areas is omitted. PE: Prediction error. KLD: Kullback-Leibler divergence between the posterior and the prior of latent variable.



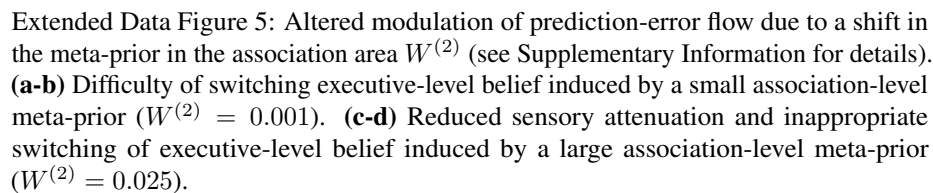
Extended Data Figure 2: Online inference in the test phase. The recurrent network updates the posterior ($z_{t-H+1:t}^{(1),q}$, $z_{t-H+1:t}^{(2),q}$, and $z_{t-H+1:t}^{(3),q}$) via minimization of the free-energy over a certain time window (H). Synaptic weights are fixed. For simplicity, the distributed structure of sensory areas is omitted.

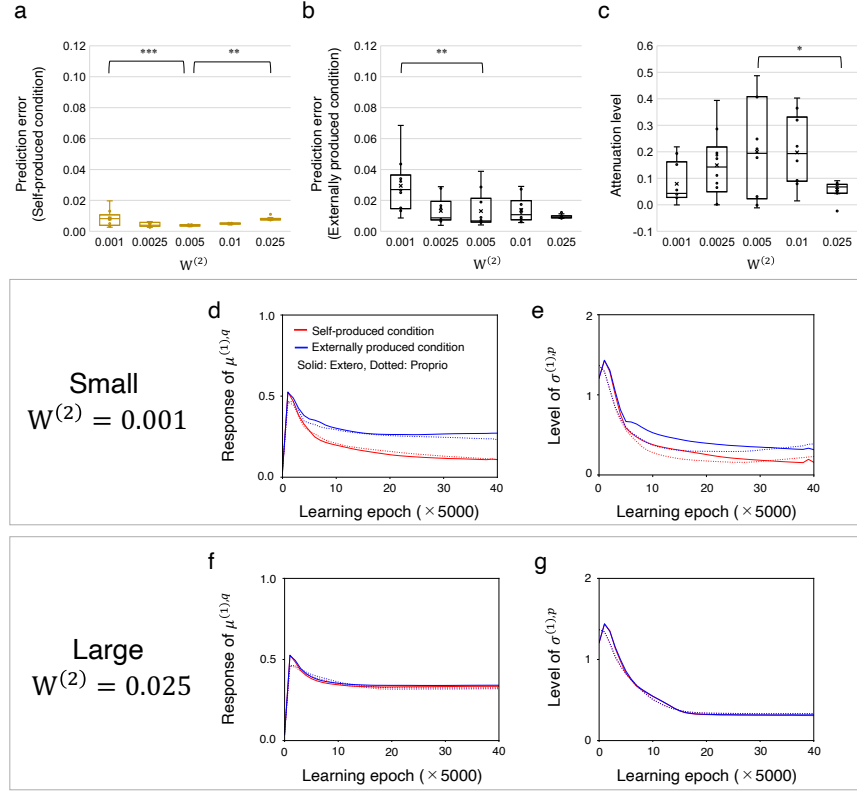


Extended Data Figure 3: Development of higher-level latent variables. **(a-b)** Development of a posterior response and a prior sigma in the association area. At each learning epoch, the value is averaged over 200 time steps, 24 training datasets, and 10 networks. **(c)** Development of the difference between self-produced conditions and externally produced conditions in the executive area. In the learning phase, the recurrent network developed a posterior state in the executive area for each of 48 training datasets (24 for self-produced conditions and 24 for externally produced conditions). The figure shows the distance between median values of posterior states for self-produced and externally produced conditions. At each learning epoch, the value is averaged over 10 networks. **(d)** An example of development of the executive-level posterior. Each figure shows the distribution of 24 executive-level posterior states corresponding to self-produced or externally produced conditions. The figure shows that recognition of different sensorimotor experiences was gradually developed through a learning process. Note that we did not provide any explicit label indicating the difference between the two conditions.

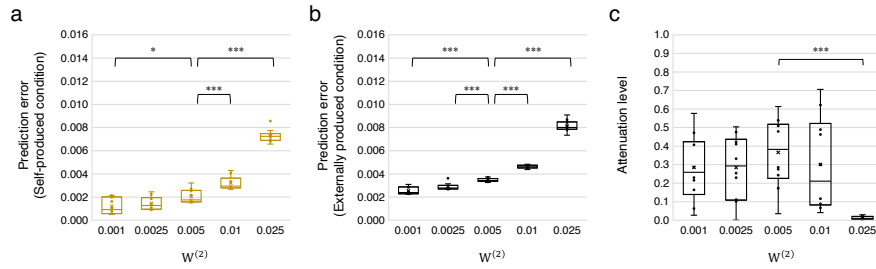


Extended Data Figure 4: Neural-response attenuation varying with the number of latent neurons. The attenuation level was calculated by subtracting the sensory-level posterior response in a self-produced condition from that in an externally produced condition while reproducing training data. Values were for 10 trained networks with different initial synaptic weights. **(a)** A larger number of association-level latent neurons led to a larger attenuation level, suggesting that representing sensorimotor correlation required enough association-level latent neurons. **(b)** When there were no executive-level latent neurons, the attenuation level was greatly reduced. This suggests the importance of executive-level control for sensory attenuation. In (a) and (b), the setting of 3 association-level and 1 executive-level latent neurons was the same baseline model.

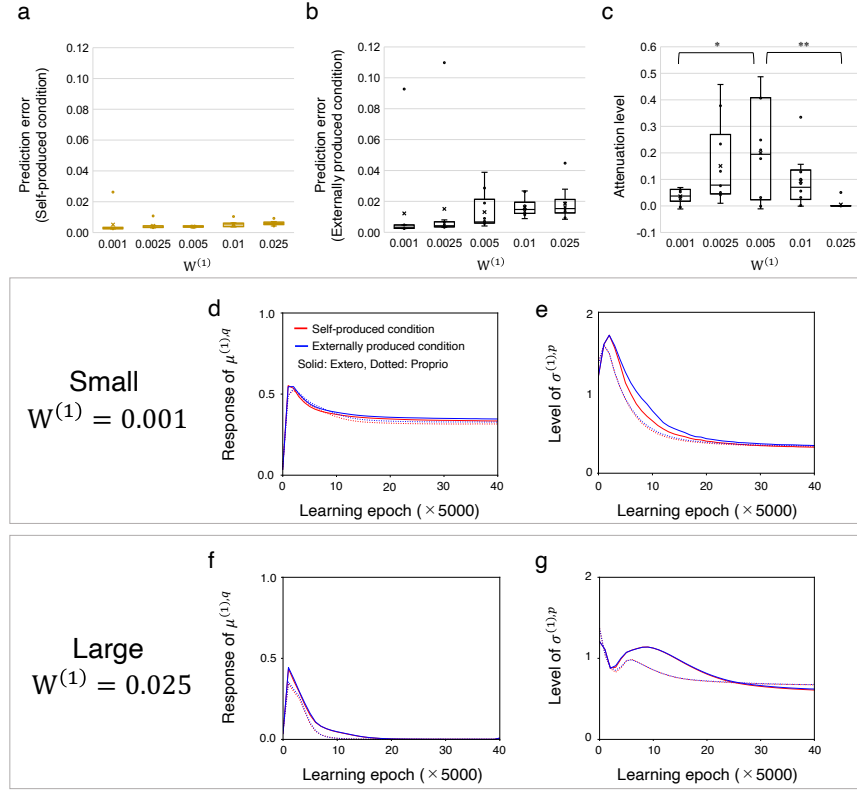




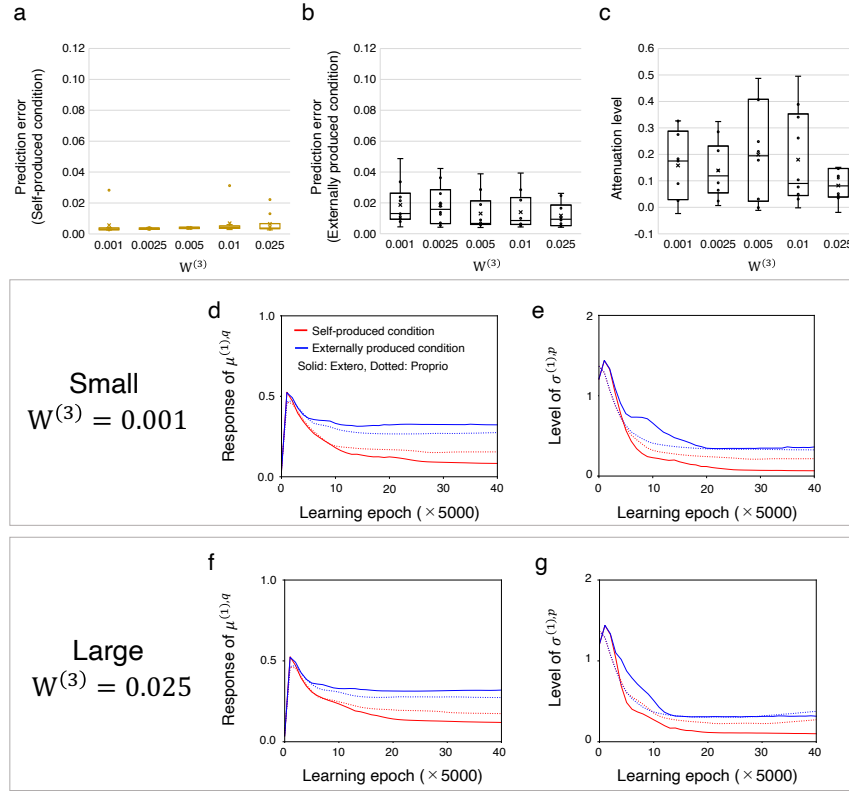
Extended Data Figure 6: Quantitative analysis for effects of a shift in the association-level meta-prior (see Supplementary Information for details). **(a-b)** The prediction error for the self-produced or externally produced condition in the test phase. In (a) and (b), each plot is an average of 100 time steps, 5 sensory dimensions, and 8 test trials by each of 10 trained networks. **(c)** The attenuation level of the sensory-level posterior response in the test phase. Each plot is an average of 2 sensory areas and 8 test trials by each of 10 trained networks. $*p < 0.05$, $**p < 0.01$, $***p < 0.001$. **(d-e)** Development of a sensory-level posterior response and prior sigma through learning in a small association-level meta-prior setting ($W^{(2)} = 0.001$), described as in Fig. 4c-d. **(f-g)** Development of a sensory-level posterior response and a prior sigma in a large association-level meta-prior setting ($W^{(2)} = 0.025$).



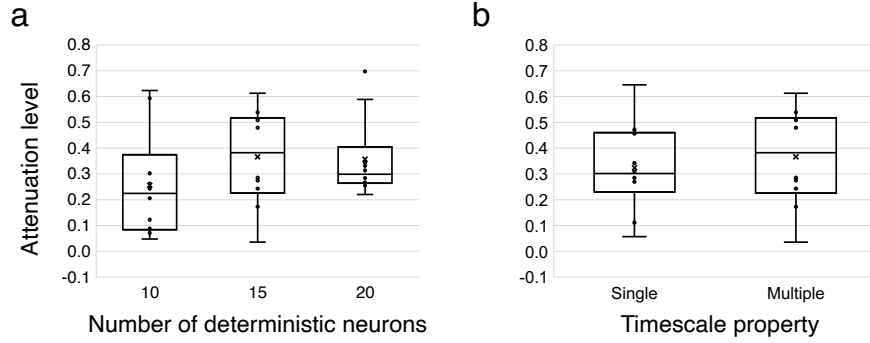
Extended Data Figure 7: Training results. **(a)** The prediction error for training data in the self-produced condition. One-way ANOVA reported a significant difference among the five meta-prior settings ($F(4, 45) = 173.9, p < 0.001$). The post hoc Dunnett's test revealed a significant decrease in $W^{(2)} = 0.001$ ($p = 0.01$), but an increase in $W^{(2)} = 0.01, 0.025$ ($p < 0.001$), compared to $W^{(2)} = 0.005$. **(b)** The prediction error for training data in the externally produced condition. One-way ANOVA reported a significant difference among the five settings ($F(4, 45) = 541.2, p < 0.001$). A Dunnett's test indicated a significant decrease in $W^{(2)} = 0.001, 0.0025$ ($p < 0.001$), but an increase in $W^{(2)} = 0.01, 0.025$ ($p < 0.001$), compared to $W^{(2)} = 0.005$. **(c)** Attenuation of the sensory-level posterior response for training data. One-way ANOVA reported a significant difference among the five settings ($F(4, 45) = 5.842, p < 0.001$). A Dunnett's test indicated a significant decrease in $W^{(2)} = 0.025$ compared to $W^{(2)} = 0.005$ ($p < 0.001$) while the difference between $W^{(2)} = 0.001$ and $W^{(2)} = 0.005$ was small ($p = 0.7$). * $p < 0.05$, *** $p < 0.001$.



Extended Data Figure 8: Effects of a shift in the sensory-level meta-prior, described as in Extended Data Fig. 6. **(a-b)** One-way ANOVA reported no significant differences in either prediction error for the self-produced condition ($F(4, 45) = 0.56, p = 0.69$) or the externally produced condition ($F(4, 45) = 0.14, p = 0.97$). **(c)** Both small and large sensory-level meta-priors led to deficits in attenuation of the sensory-level posterior response in the test trial. One-way ANOVA reported a significant difference in the attenuation level among the five levels of the sensory-level meta-prior ($F(4, 45) = 4.57, p = 0.0035$). The post hoc Dunnett's test revealed that attenuation levels were significantly lower in $W^{(1)} = 0.001$ ($p = 0.012$) and $W^{(1)} = 0.025$ ($p = 0.0023$) compared to the baseline model $W^{(1)} = 0.005$. * $p < 0.05$. ** $p < 0.01$. **(d-e)** A small sensory-level meta-prior ($W^{(1)} = 0.001$) led to reduced attenuation of the sensory-level posterior response, as well as the sensory-level prior sigma, in the self-produced condition. **(f-g)** A large sensory-level meta-prior ($W^{(1)} = 0.025$) led to highly reduced sensory-level posterior responses in both the self-produced and externally produced conditions.



Extended Data Figure 9: Effects of shifts in the executive-level meta-prior, described as in Extended Data Fig. 6. **(a-b)** Shifts in the executive-level meta-prior did not significantly affect either prediction error in the self-produced condition ($F(4, 45) = 0.69, p = 0.61$, one-way ANOVA) or the externally produced condition ($F(4, 45) = 0.74, p = 0.57$, one-way ANOVA) in the test trial. **(c)** Shifts in the executive-level meta-prior had no significant influence on attenuation of the sensory-level posterior response in the test trial ($F(4, 45) = 1.05, p = 0.39$, one-way ANOVA). **(d-g)** Neither small ($W^{(3)} = 0.001$) nor large ($W^{(3)} = 0.025$) executive-level meta-priors had a large impact on development of the sensory-level posterior response or the prior sigma.



Extended Data Figure 10: Neural-response attenuation varied with settings of deterministic neurons. The attenuation level was calculated by subtracting the sensory-level posterior response in the self-produced condition from that in the externally produced condition while reproducing training data. Values were for 10 trained networks with different initial synaptic weights. **(a)** A recurrent network with 15 deterministic neurons showed the largest average (and median) attenuation level. **(b)** Multiple timescale settings ($\tau = 2$ for 8 neurons and $\tau = 4$ for 7 neurons) increased the attenuation level compared to the single timescale setting ($\tau = 2$ for all deterministic neurons). In (a) and (b), the setting of 15 deterministic neurons and multiple timescale property was the same as the baseline model.